Photometric Repeatability and Sensitivity Evolution of WFC3/IR

D. Som, V. Bajaj, J. Mack, A. Calamida

May 24, 2021

ABSTRACT

We use spatial scanning observations of stars in the open cluster M35 to estimate the photometric repeatability of the Wide Field Camera 3 IR imaging mode and probe the time dependence of its sensitivity. With data taken using the WFC3 infrared detector and the F140W filter, we estimate the near-term 1-σ photometric repeatability to be 0.65 % and find a long-term sensitivity evolution at the rate of -0.024 ± 0.008 % per year. Our observations with the F098M filter do not suggest any significant loss of sensitivity over time but additional data are required to reach more robust conclusions. We also investigate various possible systematics affecting these analyses.

1 Introduction

The infrared channel of the Wide Field Camera 3 (WFC3/IR) on board the Hubble Space Telescope, with its full complement of 15 narrow, medium, and broad band filters and 2 grisms (G102, G141), is used heavily for a multitude of science applications: ranging from the study of the solar system to star formation, galaxy evolution and cosmology. Continued optimal and scientifically important usage of this observing mode is, therefore, critically contingent upon the characterization and monitoring of the detector stability, both in terms of short-term repeatability of photometric measurements and long-term time-dependence of detector sensitivity.

The performance of the WFC3/IR channel has been monitored, since the time of commissioning in 2009, through a body of work primarily utilizing aperture photometry of spectrophotometric stars observed in the traditional 'staring mode'. The earliest of these, incorporating the first 1.5 years of data, was presented in Kalirai, *et al.* (2011), and reported a

short-term 1-σ photometric repeatability of $\gtrsim 1$ % but no overall sensitivity evolution. A recent analysis (Bajaj, *et al.* 2020) of standard star data in various non-grism filters collected until August 2020 reports very similar findings and argue that the observed restriction of ~ 1 % in the repeatability of photometric measurements could drown out subtle trends in long-term sensitivity loss. On the other hand, a recent study (Kozhurina-Platais & Baggett, 2020) analyzing F160W observations of the stars in the core of the globular cluster ω Cen via PSF photometry found ~ 0.2 % sensitivity loss per year. Similar long-term sensitivity evolution was reported by Bohlin & Deustua (2019) using G102 and G141 observations where they found ~ 0.17 % and ~ 0.09 % per year sensitivity loss with G102 and G141, respectively.

One of the most important factors limiting studies of WFC3/IR photometric stability is the precision of individual measurements. To achieve improved precision, recent photometric calibration attempts have been focussing on the spatial scanning technique. This mode, by letting the target drift slowly across the detector during an exposure, spreads out photons from the target stars over the scan length, and thus allows the collection of a large number of photons from the relatively bright standard stars without causing significant saturation. This in turn increases the measurement precision by reducing the Poisson noise. The average over a large number of pixels also helps to minimize systematic uncertainties arising from flat fielding limitations (McCullough & MacKenty, 2012).

Here we present spatially scanned F140W photometry of stars in M35 along with a preliminary analysis of similar observations with F098M, to investigate the time-dependance of WFC3/IR sensitivity. This report is structured as follows: Section 2 describes the data used in this work while the analysis methods are described in Section 3. Section 4 presents and discusses the results of this analysis, and finally, the work is summarized in Section 5 which also includes a discussion on future work.

2 Data

This work analyzes spatial scanning observations of stars in the open cluster M35, obtained as part of calibration programs 14020 and 16031. Open clusters are groups of loose stars including photometrically stable main sequence stars that can be observed simultaneously in a single pointing and are optimal targets to investigate detector stability. Moreover, these clusters, unlike globular clusters, present relatively less crowded target fields which are more convenient for the spatial scanning technique. The data from 14020, obtained with F140W, are distributed over 4 epochs between January - April 2015 with a cadence of $\sim$1 month between the successive 1-orbit visits. The same field within M35 was targeted by program 16031 over 2 visits, each containing an orbit with F140W and F098M observations, and executed 1 year apart in January 2020 and January 2021. For both programs, each exposure, irrespective of the filter, was spatially scanned forward at 0.76 degrees and at a rate of 1.5 arcsec/sec and was ~ 8.8 sec long (`SAMP-SEQ=SPARS10, NSAMP=2`). All the observations used the same `512 x 512` sub-array readout centering on the IR detector.

The F140W data, distributed over 6 epochs between 2015 and 2021, provide a $\sim$ 6-year baseline for our analysis. The only difference in the observation structure between the two programs is in the extent of dithers; the pattern used in the last two epochs samples the
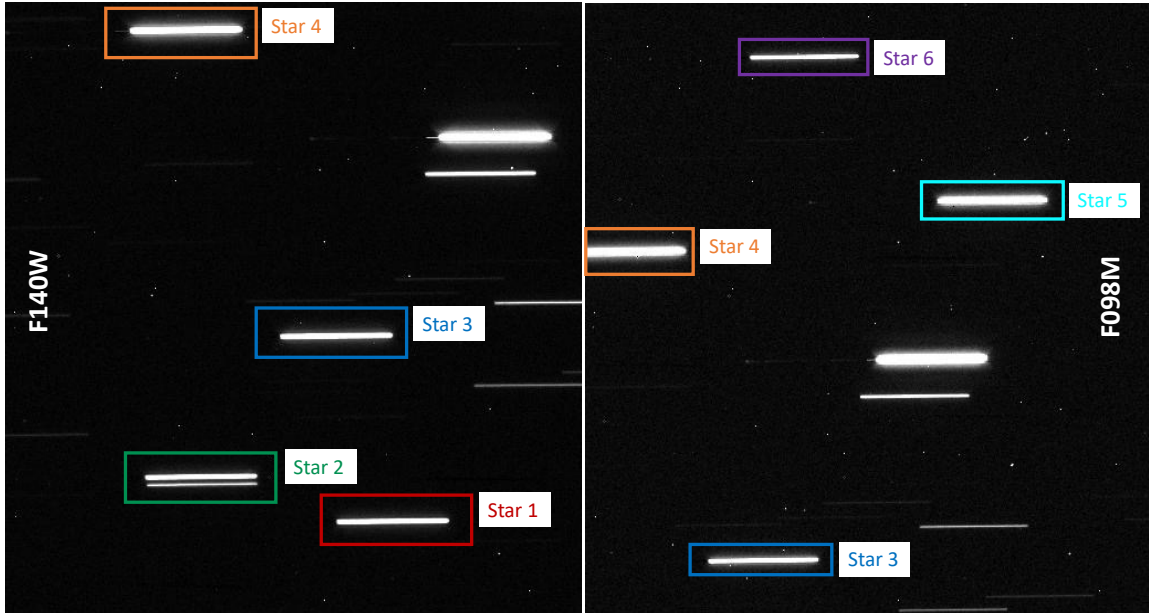
Figure 1: *Left: M35 stellar scans used in the analysis of the F140W photometry. Right: M35 stellar scans used in the analysis of the F098M photometry. Note the different sets of scans used for the analysis of F140W and F098M data, with 'Star 3' and 'Star 4' being common to both sets.*

detector more extensively and results in the scans spanning a larger footprint on the detector compared to the 2015 data. The F098M data, coming from the two visits in program 16031, provide a shorter baseline of 1 year. Our data include scans from several stars with the number varying between exposures as a result of dithering. However, for each filter, we identified a set of 4 stars (see Fig. 1) having the highest number of complete scans in our full dataset and only include them in our analysis. This results in different sets of stellar scans analyzed for F140W and F098M, with only 2 stars common between them.

3 Photometry of Spatial Scans

At the heart of this analysis lies aperture photometry of stellar scans and estimating how the measurements evolve with time. This process essentially involves measuring the flux in a scan from a given star using a rectangular aperture and determining relative photometry of a given star normalized by the mean of all measurements from that star across different epochs. Each aperture is also accompanied by a rectangular annulus used to sample the sky-background. The calibration pipeline, `calwf3 v3.5`, was used in conjunction with latest reference files including recently updated flatfields (`PFLT` and `DFLT` files, see Mack et al. 2021, and Olszewski & Mack, 2021, in prep) to process the raw data, and the pipeline-generated `IMA` files were used for our analysis. We adopt the accumulated counts from the last readout of the `IMA` files instead of the count-rates from the `FLT` files because the up-the-

ramp fitting could be sensitive to non-uniformity in scan rates and may not be accurate. Our entire analysis workflow is based on `Python 3` and utilizes packages and modules such as `astropy`[1], `photutils`[2], and `wfc3_photometry`[3]. An outline of the various steps and aspects of our analysis is given below.
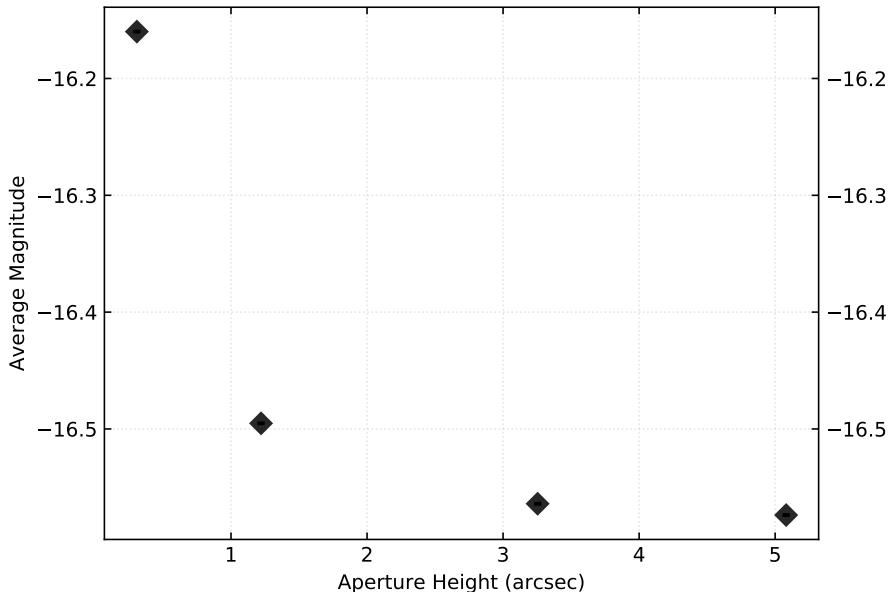
3.1 Aperture Definition

Figure 2: *Dependence of measured flux on aperture size for a stellar scan in F140W. Measured flux initially increases with increasing aperture height (across the scan), for a fixed aperture width (along the scan), before stabilizing when the width is large enough.*

Constructing apertures around the scans is the first step in the process and involves two aspects: (a) centering a scan within the aperture and (b) optimizing the aperture size so that the scan is fully contained yet the aperture is not too large to introduce additional noise. While manually centering all apertures in each image ensures the best accuracy, it could be tedious when dealing with a large number of images. We adopted an automated aperture centering strategy which involves centering the apertures in pixel space (around the 4 stellar scans used) using a reference image, converting the center locations into RA and Dec coordinates via the reference image's `WCS` information, and finally, positioning these apertures on any other image by converting the RA and Dec coordinates back into pixel space via

---

[1]The Astropy Collaboration et al. (2018). "The Astropy Project: Building an inclusive, open-science project and status of the v2.0 core package". In: ArXiv e-prints. arXiv: 1801.02634 [astro-ph.IM].

[2]Bradley, L. et al. (2017). astropy/photutils: v0.4. doi: 10.5281/zenodo.1039309. url: https://doi.org/10.5281/zenodo.1039309

[3]https://github.com/spacetelescope/wfc3_photometry

the second image's `WCS` information. This technique could result in small offsets coming from `WCS` mismatch between images but should not affect flux measurements provided the apertures are not too tightly fit around the scans. We compared measurements made using this automated technique with those from a smaller set of images using manual centering and found no significant difference.

Star	F140W Apertures		F098M Apertures	
	Width	Height	Width	Height
	(arcsec)	(arcsec)	(arcsec)	(arcsec)
1	15.25	4.75	...	...
2	15.25	4.75	...	...
3	16.00	5.00	15.50	4.75
4	17.00	5.50	16.00	5.50
5	...	...	16.00	5.25
6	...	...	15.00	4.00

Table 1: *Aperture dimensions used for measuring stellar scans from the F140W and F098M data used in this work.*

We compared flux measurements using various aperture sizes to determine the optimum aperture dimensions for measuring a given stellar scan. When the apertures are too small, the flux increases with aperture size but stabilizes to a maximum when the scan is fully enclosed. Further increase in aperture size could increase noise and/or introduce contamination from other sources. Figure 2 demonstrates this process with an aperture around a scan in F140W data, for various heights (perpendicular to scan direction) and a fixed width (along the scan). Table 1 lists the aperture dimensions, determined separately for each stellar scan in a given filter, used in the final analysis. The annular apertures used to sample background are also tailored for each star and have the same centers as the corresponding scan apertures. Their dimensions are chosen to provide a large enough area to measure the local background without getting contaminated by other sources. Since all observations used in this work use the same scan rate and exposure time, we ensure measurement consistency by using the same aperture dimensions to measure a given star in all images from the same filter. Figures 3a and 3b show the apertures and the corresponding background regions used to analyze F140W and F098M data, respectively.

The parameters for an aperture or a background region, determined as described above, were passed to `photutils` to create appropriate 'aperture objects', which then were used to perform photometry on the images.

3.2   Flux Measurement and Background Subtraction

The input data for our analysis were the last readouts of the `IMA` files. These images were first corrected for geometric distortions by multiplying with the WFC3/IR pixel-area map: '`ir_wfc3_map.fits`' [4]. The apertures defined above were then used to measure fluxes

---

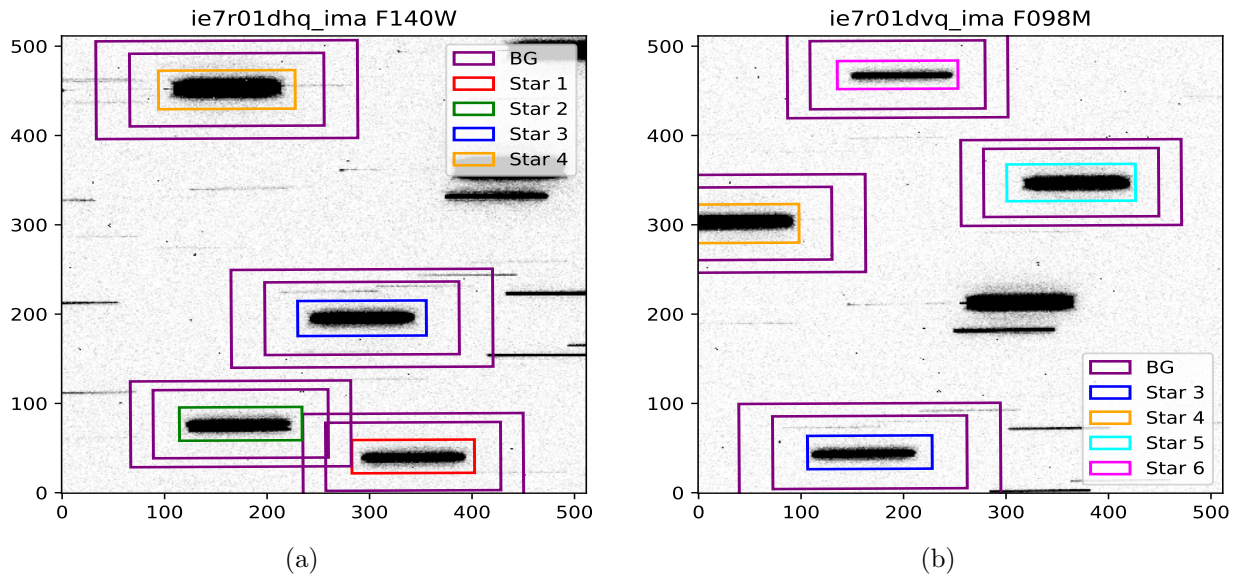[4]https://www.stsci.edu/hst/instrumentation/wfc3/data-analysis/pixel-area-maps

Figure 3: *(a): The apertures and the corresponding background regions used for measuring the stellar scans in F140W. The aperture measuring star i is marked as 'Star i' where $i = 1, 2, 3,$ or 4. The color scheme used to mark these apertures is carried forward through the following plots presenting measurements from the corresponding stars. (b): Same as Fig. 3a but for measurements with F098M data. The aperture measuring star i is marked as 'Star i' where $i = 3, 4, 5,$ or 6. Star 3 and Star 4 are common to both filters.*

(total counts) in the scans and the corresponding Poisson errors using modules available in the `wfc3_photometry` package. The typical local background in each pixel within a given scan is estimated as the mean pixel value within the corresponding background aperture. The total background in the measured flux is then calculated by scaling this value by the area of the photometric aperture and the corresponding error is estimated as well. This background is then subtracted from the measured flux to obtain the corrected photometry and the errors are propagated appropriately. A median statistic in estimating the typical background would be more outlier (contamination) resistant than the mean. However, in practice, the fraction of contaminated pixels within the background aperture is typically very small and therefore, using the mean background should result in similar measurements as using the median background. Indeed, our tests using these two statistics on a random subset of data produced mutually consistent results.

Because of dithering, a given stellar scan can fall on different parts of the detector and can even be cut-off by detector edges. Therefore, as a final step, the measurements are filtered to discard scans which are only partially covered by the detector or are so close to the edges that significant fractions of their background apertures are lost. This is achieved by rejecting apertures with centers within ∼30 (60) pixels of the left/right (top/bottom) edges. These 'buffer' regions were estimated based on the typical scan length and/or background region dimensions.

4   Results and Discussions

We combine measurements from different epochs and investigate short and long term photometric stability of the WFC3/IR imaging mode. This is achieved by studying how the relative photometry of the stars in our sample, obtained by normalizing the individual measurements from a star by the mean of all its measurements from a given filter, vary across time. The results from this study are given below.

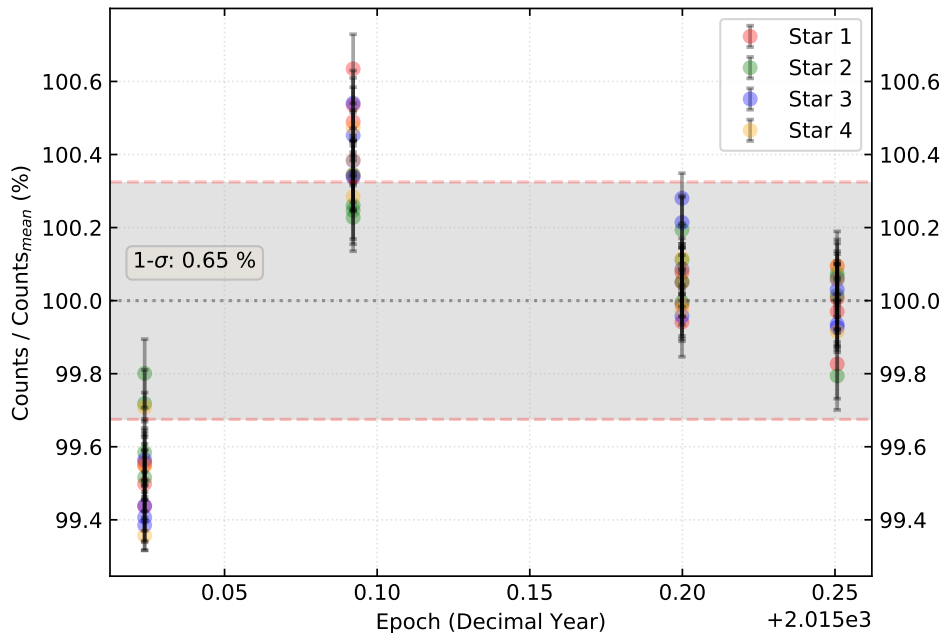## 4.1   Photometric Repeatability

Figure 4: *Estimation of photometric repeatability with WFC/IR using 4 epochs of F140W observations from program 14020. Measurements from each star, plotted relative to their mean over all four visits, are plotted against time while the mean photometry is represented by the black dotted line at 100%. The 1-σ repeatability, derived by scaling the standard deviation in the measurements by a factor of 2, is shown by the grey shaded region between the red dashed lines.*

We consider observations from program 14020, taken with F140W over four epochs each ~ 1 month apart, to determine the extent to which the photometric measurements are repeatable. This is essentially an estimation of the scatter in measurements made at different points in time and could involve observations from the same orbit as well as from different orbits and visits. The time interval used for this repeatability measurement can be arbitrarily large in the absence of an overall sensitivity evolution. However, when a long-term evolution is present, the repeatability measured over a long interval can capture this evolution if appropriate corrections are not applied. The time interval chosen for our analysis is short enough, given the rate at which the sensitivity is found to evolve (see Section

4.2), to estimate the repeatability in the short-term without any significant contamination from the long-term evolution. Figure 4 shows relative photometry of our target stars over time between January and April in 2015, and the measurements, on average, are found to be repeatable within ~ 0.65 %. We note that this 1-σ repeatability is lower than the > 1 % estimate reported by Kalirai, *et al.* (2011) using a baseline of ~ 1.5 years.

As seen in Figure 4, the repeatability estimate contains contributions from variations between visits as well as that within the individual 1-orbit visits. However, the scatter within a visit appears to be uniform across the visits and is described further in Section 4.3. For the remainder of this section, we will focus on the dispersion between visits. It is worth noting that most of the dispersion arises between the first and the second epoch. The heightened brightness measured from the second epoch might have been caused by the residual glow of persistence of an internal flat taken ~ 6 hours before this visit. On the other hand, the detector downtime (a measure of the length of time the detector was unused, and in autoflush mode, before a set of observations) was the longest for the first epoch which also produced the lowest relative photometry. Therefore, an estimation of WFC3/IR photometric repeatability could be affected by systematics arising from detector illumination history, especially at the precision afforded by the spatial scanning technique. Disentangling these effects would require modeling the detector's response to previous exposures as a function of the downtime and the degree of illumination, which needs a much larger dataset and is beyond the scope of this work. We also note that the relative photometry of all the stars, as can be seen in Figure 4, exhibit the same time-dependance which rules out any peculiar variability in any of our target stars.

4.2   Time-dependence of Sensitivity

We added the F140W observations from January 2020 and January 2021 to the data used in the photometric repeatability analysis, and obtained the first estimate of the time dependance of WFC3/IR imaging mode sensitivity using the spatial scanning technique over a ~ 6 year baseline. Figure 5a shows the measurements along with a linear fit to the data. The slope indicates a loss of sensitivity in F140W at the rate of 0.024 ± 0.008 % per year. This rate is lower than that reported for staring mode observations: globular cluster data in F160W (Kozhurina-Platais & Baggett, 2020) as well as CALSPEC (grism modes; Bohlin & Deustua, 2019). The weak loss in sensitivity as measured via spatial scans is more consistent with the results from staring mode standard star data observed with non-grism filters (Bajaj, *et al.* 2020). We note that our reported rate of sensitivity evolution is $\sim 3\sigma$ significant and a more detailed description of this evolution requires more data over a longer baseline.

We also investigated the time-dependance of sensitivity in F098M using observations from the two visits in 16031, and found no significant sensitivity evolution (estimated rate of -0.044 $\pm$ 0.070 % per year, see Figure 5b) with the precision afforded by the current data. We note that sensitivity evolution in F098M is rather inconclusive owing to the limited data volume as well the shorter baseline in comparison with F140W and we stress that more observations with F098M over a longer time interval are required to reach more robust conclusions.
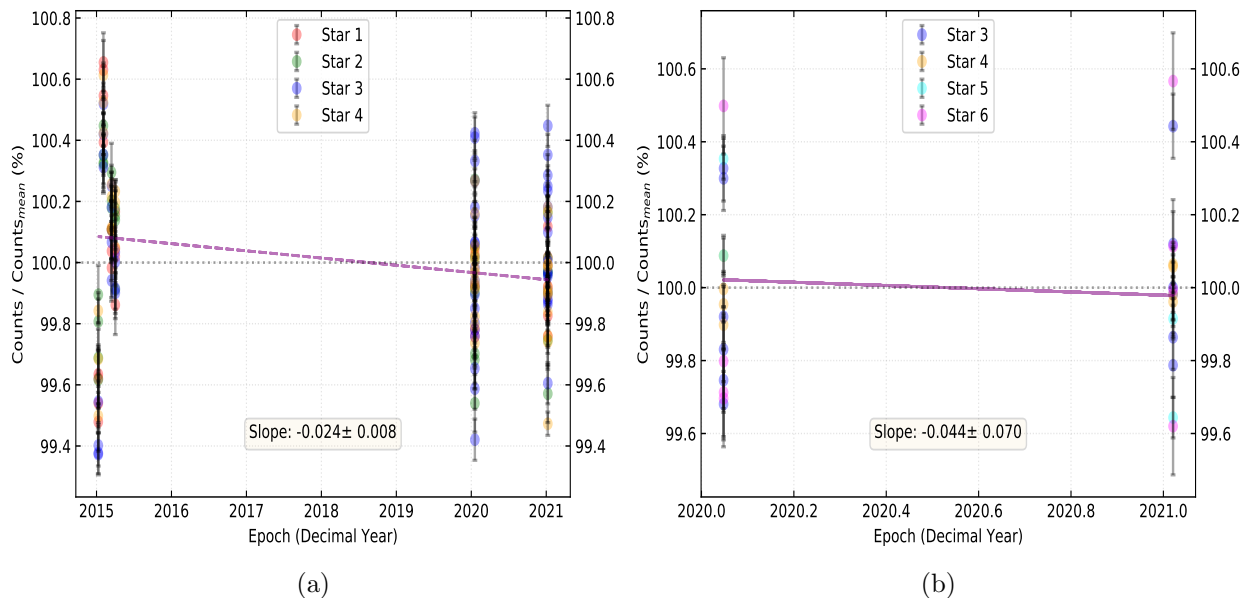
Figure 5: *(a): Estimation of the time dependence of WFC3/IR imaging mode sensitivity using spatial scanning observations with F140W from programs 14020 (4 visits in 2015) and 16031 (2 visits in January 2020 & January 2021). Measurements from each star, plotted relative to the mean over all six epochs, are plotted against time. The mean photometry is represented by the level at 100% (black dotted line). The solid purple line represents a liner fit to the data. The corresponding slope, quantifying the rate of sensitivity evolution is also shown. (b): Same as Fig. 5a, but with F098M data from the two 16031 visits in January 2020 and January 2021.*

4.3 Intra-visit Scatter in Measurements

The intra-visit scatter can be described as the scatter present in the relative photometry from all the stars in a given visit (orbit), and as mentioned in Section 4.1, constitutes a partial measure of the photometric repeatability. As seen in Figures 4 & 5a, F140W observations show intra-visit scatter at a level higher than that expected from the Poisson noise alone. Moreover, the two visits in 16031 show a considerably higher degree of scatter compared to the earlier visits. We investigate this issue further as this scatter, as part of the short-term photometric repeatability, can potentially limit the precision with which the long-term time-dependent sensitivity of WFC3/IR imaging mode can be measured.

While the other parameters were identical between the programs, the observations in 16031 employed a more extensive dither pattern compared to that in 14020, leading to a larger footprint of the stellar scans over the detector. Indeed, the level of dispersion in measurements appears to correlate with the extent of dithering. The two visits in 16031 were identical in structure and show very similar levels of scatter. Furthermore, Figure 6a shows only those measurements from 16031 which match the dither positions used in 14020 and the resulting intra-visit scatter appears to be similar across all epochs. This positional dependence of measurements led us to investigate systematic effects such as the possible brightening of stellar scans located near the center of the detector, due to read-out delay,

9

but these systematics were found to be too small to account for the observed scatter.
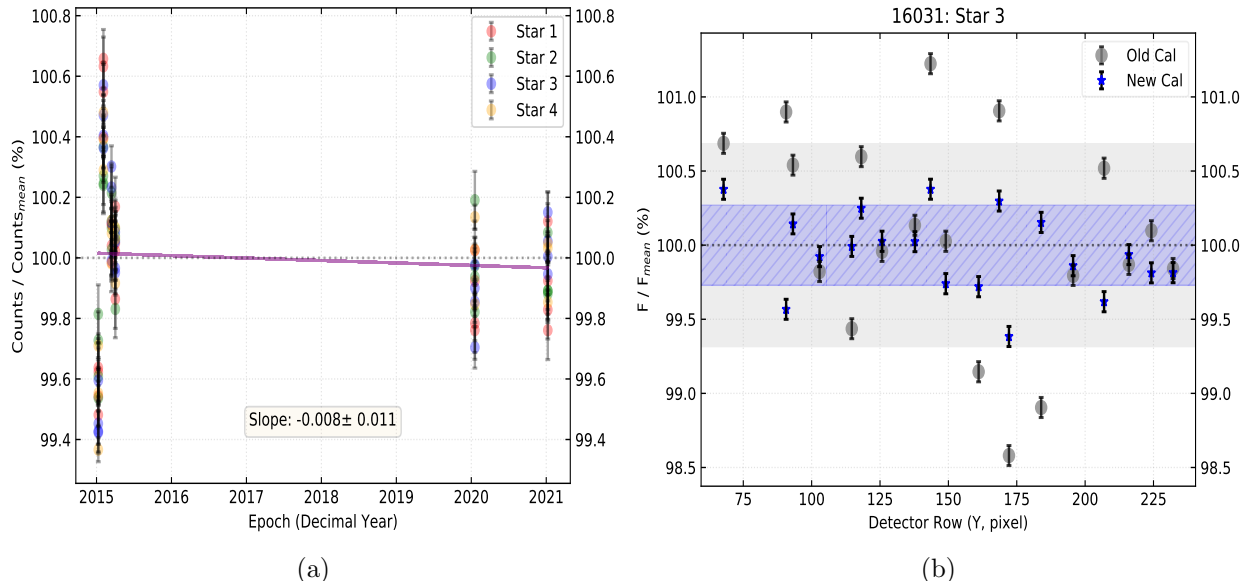

(a) (b)

Figure 6: *(a): Same as Fig. 5a, but only data from 16031 matching the dither positions used in 14020 were included. (b): Effect of flat-fielding improvement on measurements from Star 3 (having the most extensive footprint across the detector) scans located on various parts of the detector. All measurements come from F140W observations in program 16031. Measurements on data processed using less accurate flats are shown in grey and the corresponding scatter of ~ 1.36 %, estimated by doubling the standard deviation of the measurements, is represented by the grey shaded region. Measurements reflecting the latest improved flats are shown in blue and their scatter, at ~ 0.54 %, is represented by the blue shaded region.*

Since it depends on the extent of scan footprint across the detector, the increased scatter could possibly be driven by limitations in the flat-fielding accuracy. To investigate the effect of flat-fielding on measurement dispersions, we compared our analysis with that using an older set of less accurate flats and, as shown in Figure 6b, found the improved flatfields to reduce the scatter by ~ 60 %. However, this effect diminishes in the case of data from 14020 which had a less extensive dither pattern across the FOV. Thus the degree of reduction in scatter with improved flat-fielding accuracy seems to depend on the extent of dithering. It is, therefore, likely that the current maximum intra-visit scatter of ~ 0.5 % in the spatial scanning photometric measurements is mostly probing large scale flat-field inaccuracies.

5   Summary

The work presented here addresses the issue of estimating photometric stability of WFC3/IR which is of critical importance in supporting a wide range of science applications. Our work investigates both short and long term photometric stability of the WFC3/IR imaging mode utilizing, for the first time, high-precision photometry derived from spatial scanning observations. Our data, comprising F140W observations of stars in the open cluster M35, span 4

visits in 2015 (cadence of $\sim$ 1 month between successive visits) and 2 visits (1 year apart) between 2020 - 2021. The later two visits also include F098M observations. We estimate a short term photometric repeatability of 0.65 % using F140W observations spanning a $\sim$ 4 months baseline and argue that this estimate could be dominated by systematics arising from detector response to illumination history. The intra-visit (1 orbit) scatter in photometry, as revealed by F140W observations, can reach up to $\sim$ 0.5 % and is found to depend on the extent of dithering, and we argue that this scatter may be connected to flat-fielding accuracy. We also find the WFC3/IR sensitivity in F140W to be evolving with time at a rate of -0.024 $\pm$ 0.008 % per year. While our preliminary investigation with a limited F098M dataset does not find any significant evidence of sensitivity evolution, we highlight the need for more observations, over a longer baseline, to arrive at more robust conclusions. Looking ahead, we plan to add more observations across various filters to better understand the photometric stability of WFC3/IR imaging mode using the spatial scanning technique.

6 Acknowledgements

References

Bajaj, V. (2020). "Updated WFC3/IR Photometric Calibration." WFC3 ISR 2020-10.

Bohlin, R. C. & Deustua, S. E. (2019). "CALSPEC: Wide Field Camera 3 Infrared Grism Spectrophotometry." AJ, 157, 229.

Kalirai, J. et al. (2011). "The Photometric Performance of WFC3/IR: Temporal Stability Through Year 1." WFC3 ISR 2011-08.

Kozhurina-Platais, V. & Baggett, S. (2020). "WFC3 IR sensitivity over time." WFC3 ISR 2020-05.

Mack, J., Olszewski, H. & Pirzkal, N. (2021). "WFC3/IR Filter-Dependent Sky Flats." WFC3 ISR 2021-01.

McCullough. P. & MacKenty, J. (2012). "Considerations for using Spatial Scans with WFC3." WFC3 ISR 2012-08.

Olszewski, H. & Mack, J. (2021), "WFC3/IR Blob Flats." in prep.